Solid Earth Discuss., https://doi.org/10.5194/se-2017-112
Manuscript under review for journal Solid Earth
Discussion started: 10 October 2017

Controls on fault zone structure and brittle fracturing in the foliated hanging-wall of the Alpine Fault

Jack N. Williams[a]*, Virginia G. Toy[a], Cécile Massiot[b,c], David D. McNamara[c,e], Steven A. F. Smith[a], Steven Mills[d]

Affiliations:

[a]Department of Geology, University of Otago, PO Box 56, Dunedin 9054, New Zealand

[b]School of Geography, Environment, and Earth Sciences, Victoria University of Wellington, PO Box 600, Wellington 6012, New Zealand

[c]GNS Science, PO Box 30-368, Lower Hutt 5040, New Zealand

[d]Department of Computer Science, University of Otago, PO Box 56, Dunedin 9054, New Zealand

[e]Department of Earth and Ocean Sciences, NUI Galway, University Road, Galway, Ireland

***Corresponding Author:** Jack Williams[a] (email: jack.williams@otago.ac.nz)

Abstract

The orientations and densities of fractures in the foliated hanging-wall of the Alpine Fault provide insights into the role of a mechanical anisotropy in upper crustal deformation, and the extent to which existing models of fault zone structure can be applied to active plate-boundary faults. Three datasets were used to quantify fracture damage at different distances from the Alpine Fault principal slip zones (PSZs): (1) X-ray computed tomography (CT) images of drill-core collected within 25 m of the PSZs during the first phase of the Deep Fault Drilling Project that were reoriented with respect to borehole televiewer images, (2) field measurements from creek sections at <500 m from the PSZs, and (3) CT images of oriented

Solid Earth Discuss., https://doi.org/10.5194/se-2017-112
Manuscript under review for journal Solid Earth
Discussion started: 10 October 2017

drill-core collected during the Amethyst Hydro Project at distances of ~500-1400 m from the PSZs. Results show that within 160 m of the PSZs in foliated cataclasites and ultramylonites, gouge-filled fractures exhibit a wide range of orientations. At these distances, fractures are interpreted to form at high confining pressures and/or in rocks that have a weak mechanical anisotropy. Conversely, at distances greater than 160 m from the PSZs, fractures are typically open and subparallel to the mylonitic foliation or schistosity, implying that fracturing occurred at low confining pressures and/or in rocks that are mechanically anisotropic. Fracture density is similar across the ~500 m width of the hanging-wall datasets, indicating that the Alpine Fault does not have a typical "damage zone" defined by decreasing fracture density with distance. Instead, we conclude that the ~160 m-wide zone of intensive gouge-filled fractures provides the best estimate for the width of brittle fault-related damage. This estimate is similar to the 60-200 m wide Alpine Fault low-velocity zone detected through fault zone guided waves, indicating that a majority of its brittle damage occurs within its hanging-wall.

Keywords: fractures, anisotropy, Alpine Fault, Deep Fault Drilling Project, damage zone

1. Introduction

Conceptual models of fault zone structure in the upper crust often invoke a relatively narrow "fault core" that accommodates most displacement, surrounded by a halo of heavily fractured rock termed the "damage zone" (Caine et al., 1996; Chester et al., 1993; Chester and Logan, 1986; Faulkner et al., 2010). These models have been successfully applied in a variety of tectonic settings and for a wide range of fault displacements and exhumation depths (e.g. Choi et al., 2016; Faulkner et al., 2010; Kim et al., 2004; Mitchell and Faulkner, 2009; Savage and Brodsky, 2011). However, the term "damage zone" has been applied by geologists and geophysicists to describe a range of fault-related features in a fairly inconsistent way (Choi et al., 2016; Cochran et al., 2009; Peacock et al., 2016). For example, the term has been used to describe fractures and faults at stepovers and bends (Chester and

Solid Earth Discuss., https://doi.org/10.5194/se-2017-112
Manuscript under review for journal Solid Earth
Discussion started: 10 October 2017

Chester, 2000; Kim et al., 2004; Mitchell and Faulkner, 2009; Wilson et al., 2003), the volume of inelastic deformation that is induced by dynamic off-fault stresses during fault-tip/earthquake rupture propagation (Andrews, 2005; Cowie and Scholz, 1992; Rice et al., 2005; Templeton and Rice, 2008; Vermilye and Scholz, 1998), and the volume of rock in which earthquake swarms or foreshock and aftershock sequences are localised (Kim and Sanderson, 2008; Savage et al., 2017; Sibson, 1989; Yukutake et al., 2011). Furthermore, whereas damage zones are typically reported to be <5 km in width (Faulkner et al., 2011; Savage and Brodsky, 2011), co-seismic ground shaking can modify fracture permeability at distances many hundreds of kilometres from the fault source (Cox et al., 2015; Muir-Wood and King, 1993; O'Brien et al., 2016).

Brittle faults often develop in mylonite sequences or other (e.g. jointed) rocks that contain compositional and mechanical anisotropies (Bistacchi et al., 2012; Chester and Fletcher, 1997; Massironi et al., 2011). Evidence from field studies (Bistacchi et al., 2010; Peacock and Sanderson, 1992), experiments (Donath, 1961; Misra et al., 2015; Paterson and Wong, 2005), and numerical modelling (Chester and Fletcher, 1997) demonstrates that such anisotropy can significantly affect the orientation and densities of brittle fractures. Despite this, "fault core-damage zone" models are based largely on field observations from relatively isotropic and homogenous host rocks, and there have been comparatively few field studies (Bistacchi et al., (2010) being a notable exception) that document the influence of mechanical anisotropy on patterns of brittle fracture damage in large-displacement faults.

In this contribution, we present a comprehensive study of fracture densities, orientations, and mineral fills across the hanging-wall of the Alpine Fault' central section. In doing so, we critically assess the application of "damage zone" models to a plate-boundary-scale structure. In addition, the Alpine Fault is an active fault that rapidly exhumes ductile-to-brittle fault rock sequences from depths of up to 35 km (Little et al., 2005; Norris and Toy, 2014;

Sutherland et al., 2007). Brittle fracturing in its hanging-wall therefore overprints a 1-2 km wide mylonite sequence containing a pervasive foliation sub-parallel to the main fault surface (Cooper and Norris, 1994; Norris and Cooper, 1997, 2007; Toy, 2008), which provides an opportunity to assess the influence of rock anisotropy on fracturing. Observations of fracturing have been made from multiple datasets and across a range of scales. Measurements from within 25 m of the Alpine Fault principal slip zones (PSZs) were made from shallow (depths <130 m) drill-cores and wireline logs obtained during the first phase of the Deep Fault Drilling Project (DFDP-1). These are combined with field studies at distances <500 m from the PSZs and analyses of drill-core recovered at 500-1400 m from the PSZs during the Amethyst Hydro Project (AHP). Results are then compared to geophysical studies (Boese et al., 2012; Chamberlain et al., 2017; Eccles et al., 2015) to improve our understanding of the structure of the Alpine Fault, and to provide new insights into the relationships between fracturing and mechanical anisotropy.

2. Tectonic setting of the Alpine Fault

The Alpine Fault is a crustal-scale (along strike extent ~850 km, depth ~35 km) transpressive discontinuity accommodating ~70% of Pacific-Australian plate motion in the South Island of New Zealand (DeMets et al., 1994; Norris and Cooper, 2001, Figure 1a). Slip rates vary along strike such that it can be broadly divided into three sections: (1) a northern section between Lake Rotoiti and its intersection with the Hope Fault near Hokitika, (2) a central section between Hokitika and Haast (Figure 1a), and (3) a southern section between Haast and its offshore termination near the Puysegur subduction zone (Norris and Cooper, 2007; Sutherland et al., 2007). This study focuses on the central section where the fault currently accommodates dextral strike-slip at a rate of 27 ± 5 mm/yr and dip-slip at a rate of 6-10 mm/yr (Little et al., 2005; Norris and Cooper, 2001).

Solid Earth Discuss., https://doi.org/10.5194/se-2017-112
Manuscript under review for journal Solid Earth
Discussion started: 10 October 2017

In the central section at depths greater than 8-12 km, the Alpine Fault accommodates motion via viscous creep across a >1 km wide ductile shear zone in which the hanging wall "Alpine Schist" protolith is progressively mylonitised (Norris and Cooper, 2007; Toy et al., 2010). Shear strains increase with proximity to the Alpine Fault so that a sequence of protomylonites, mylonites and ultramylonites form (Figure 2), which are exhumed to the surface in the Alpine Fault's hanging-wall (Norris and Cooper, 2003; Reed, 1964; Toy et al., 2008). Foliation in the mylonite sequence is mainly defined by alternating quartzofeldspathic layers and mica-rich layers (Figure 2). Bottle-green hornblende-rich metabasic mylonites or purple-dark grey mylonites that are comparatively mica rich are also present, and reflect variations in protolith lithology (Cooper and Norris, 2011; Norris and Cooper, 2007; Sibson et al., 1981; Toy, 2008). As the mylonite sequences are exhumed to depths of less than 8-12 km, temperatures drop below those at which quartz plasticity occurs and brittle deformation starts to overprint the mylonitic shear zone (Norris and Cooper, 2007; Toy et al., 2010, 2015). This is reflected in the formation of a ~20 m thick layer of green, indurated and frequently foliated cataclasite (Allen et al., 2017; Toy et al., 2015), and a 10-50 cm thick clay-rich principal slip zone (PSZ) that is preserved adjacent to the currently-active fault trace (Boulton et al., 2017, 2012; Ikari et al., 2014; Mitchell and Toy, 2014).

Projections of outcrop-derived measurements (Norris and Cooper, 1995, 2007) and geophysical imaging (Stern et al., 2007) indicate that at depths >4 km the central section of the Alpine Fault zone can be considered a single sub-planar structure, which is thought to have the same orientation as the regional mylonitic foliation (055/45 SE). However, at depths of less than 4 km, perturbations in the regional stress field induced by hanging-wall topography results in segmentation of the fault trace into a series of km-long, approximately E-W striking and steeply-dipping strike-slip fault strands and NE-SW striking, gently-dipping (~30º) thrust segments (Barth et al., 2012; Norris and Cooper, 1995, 2007; Simpson et al., 1994).

Solid Earth Discuss., https://doi.org/10.5194/se-2017-112
Manuscript under review for journal Solid Earth
Discussion started: 10 October 2017

3. Methodology

3.1 Fracture orientations from DFDP-1 drill-core

Hanging-wall fracture orientations at less than 25 m orthogonal distance from the PSZ were assessed through analysis of datasets arising from the first phase of the Deep Fault Drilling Project (DFDP-1, http://alpine.icdp-online.org). DFDP-1 successfully sampled the Alpine Fault in two boreholes (DFDP-1A and DFDP-1B, Figure 3) at depths of less than 150 m in early 2011 at Gaunt Creek (Figure 1b, Sutherland et al., 2012). The geophysical properties of the DFDP-1 boreholes were characterised by a full suite of wireline logs (Townend et al., 2013), which were combined with visual core descriptions to construct a lithological classification scheme for DFDP-1 drill-core (Figure 3, Toy et al., 2015).

Abundant fractures, typically with a gouge-fill, were observed in X-ray computed tomography (CT) scans of DFDP-1 drill-core (Williams et al., 2016). The true orientation of these fractures was determined for the depth interval 94-126 m in the DFDP-1B borehole (Figure 3). True fracture orientations were obtained by generating 'unrolled' CT images of individual core sections (Mills and Williams, 2017), which are directly analogous to geographically referenced - but lower resolution - borehole televiewer (BHTV) images. Where fractures could be matched between the two images, a rotation could be derived to transform all fracture orientations in the CT scans from a local core reference frame to their true geographic orientation (Figure 4). Depending on the number of fractures matched, core was rotated with a high, moderate, or low degree of confidence. A full methodology is provided in Appendix A the rotations applied to DFDP-1 core sections are listed in Table S1, and a CT-BHTV image comparison is given in Williams et al., (2017b).

Solid Earth Discuss., https://doi.org/10.5194/se-2017-112
Manuscript under review for journal Solid Earth
Discussion started: 10 October 2017

3.2 Field observations of fracture orientations and densities

At distances up to 150-250 m from the PSZs, fracture orientations and densities were measured in four creeks (Gaunt Creek, Stony Creek, Hare Mare Creek and Havelock Creek, Figure 1b) that cut across the hanging-wall mylonite sequence approximately perpendicular to the main fault trace (Figure S1). Along each creek, fracture orientations and densities were collected at 3 or 4 measuring stations. Additional information was also collected at c. 500 m from the Alpine Fault in Bullock Creek (Figure 1b). Each creek transect cuts across a thrust segment of the Alpine Fault, and thus orthogonal distance between the measuring stations and the PSZs was calculated assuming a fault dip of 30º (Norris and Cooper, 1995, 1997). The mylonite lithology for each station was classified using the scheme presented in Toy, (2008).

The density of fractures at each measuring station was calculated following the methodology of Hudson and Priest, (1983) and Schulz and Evans, (2000), where the number and orientation of fractures that intersect a linear transect was recorded. This technique has the tendency to under-sample fractures oriented sub-parallel to the scan-line. Therefore, a weighting (*w*) factor calculated using a modified version of the Terzaghi correction (Massiot et al., 2015; Terzaghi, 1965) was applied to each fracture, and results are shown as 'corrected' fracture density.

3.3 Fracture orientations and densities in the Amethyst Hydro Project boreholes

The Amethyst Hydro Project (AHP) was developed to divert water from the Amethyst Ravine down a 1040 m-long tunnel to a powerhouse on the floodplain of the Wanganui River. Prior to the main phase of tunnelling, four exploratory boreholes (BH1-4; Figure 1b and S2) were completed between 2005-2006, resulting in the recovery of a total of ~890 m of drill-core at depths of 50-200 m. The boreholes are situated 1-2 km east of the surface trace of the Alpine

Fault. Below the boreholes, the Alpine Fault dips c. 45º to the east (Norris and Cooper, 1995) meaning that drill-cores are at orthogonal distances of ~0.5-1.4 km from the PSZs.

To provide a dataset analogous to the DFDP-1 CT scans, a total of 31.9 m of drill-core from the AHP boreholes was CT scanned at the Southern Cross Hospital in Wellington, New Zealand. Initial descriptions of the drill-core found that the Rock Quality Designation (RQD, the % of intact core lengths >100 mm/1 m of drill-core) varied considerably. Intervals with RQD values less than 10% are related to intense fracturing adjacent to the Tarpot Fault and other minor faults that intersect the AHP boreholes (Geotech Consulting Limited, 2006; Savage, 2013, Figure S3). To ensure that the description of the fracture network sampled in the AHP is unaffected by damage from these minor faults, CT scanning was focussed on intervals of high RQD (Figure S2). The CT scanner was operated at 100 mA and an X-ray tube voltage of 120 kVp. Slice spacing was 1.25 mm, field of view 250 mm, and the image size was 512 x 512 pixels. Therefore, the size of one voxel is 0.488 x 0.488 x 1.25 mm in the x, y, z directions respectively. Reconstruction of two-dimensional CT slices into three-dimensional images of the drill-core was performed using OsiriX Imaging Software (http://www.osirix-viewer.com/).

AHP drill-core was not oriented. However, the prominent schistosity observed in the drill-cores has a known orientation and can be used as a reference to reorient drill-core back into a geographic reference frame. For BH2 and BH3 drill-cores, which are vertical, this required only a single transformation. For the inclined BH1 and BH4 drill-cores, this required first rotating the core with respect to the foliation. These orientations were then corrected for the inclination of the drill core using the Planes from Oriented and Navigated Drillcore (POND) Excel spreadsheet (Stanley and Hooper, 2003).

4. Results

4.1 Fracture orientations in DFDP-1 drill-core within 25 m of the Alpine Fault

In the DFDP-1 CT images, a total of 637 fractures were rotated into their true geographic orientation (Figure 5a; Appendix B). In both the CT and BHTV datasets, a set of fractures is observed sub-parallel to the mylonitic foliation and Alpine Fault orientation at Gaunt Creek (015/43 E, Figures 5a and b; Townend et al., 2013). Clustering of this fracture set is stronger in the lower-resolution BHTV images indicating that: (1) fractures observed at the resolution of the BHTV are more likely to be aligned subparallel to the fault plane and foliation than those visible in CT, and/or (2) some of the planar structures identified from the BHTV images were the mylonitic foliation itself. The comparison between CT and BHTV images is discussed further in Appendix B.

No clear relationships are generally observed between the type of fracture (Williams et al., 2016) and fracture orientation (Figure 5a). Plotted separately in Figures 5c and 5d are fractures hosted in foliated ultramylonites and cataclasites (Units 1, 2 and 4 of Toy et al., 2015) and fractures hosted in relatively homogenous unfoliated cataclasites (Unit 3 of Toy et al., 2015). It is evident that fractures in the foliated units are more clustered around the local Alpine Fault and foliation orientation than fractures in the homogenous units. However, even within the foliated units there are many fractures that cut across the foliation at a wide range of orientations (Figure 5c and 6).

4.2 Fracture orientations, densities, and fill in field transects within 500 m of the Alpine Fault

The orientations and densities of fractures observed in the four-main field transects are summarised in Figure 7. In these transects, similar structures to those observed in the CT scans of DFDP-1 core are identified (Figure 8). Total fracture density in the transects varies between 3-30 fractures/metre, and there are no clear decreases in fracture density with increasing distance from the Alpine Fault in any of the transects (Figure 7a). Distinctive gouge-filled fractures (Figure 8a-c) are observed at all distances from the Alpine Fault, but are relatively abundant (>1 fracture/metre, Figure 7a, Table S2) only within approximately 100-160 m of the PSZs (Figure 7a). The thicker gouge-filled fractures (> 1cm) commonly juxtapose different lithologies or offset markers (Figure 8g-i). Thinner gouge-filled fractures (< 1cm) are localised within 160 m of the Alpine Fault. Open fractures (Figure 8d-f) are present at all stations, though are most prevalent at those furthest from the fault (Figure 7b).

The composition of the mylonites can also affect fracture density. Intervals of micaceous mylonites and ultramylonites are observed to contain relatively high densities of gouge-filled fractures when they are juxtaposed against quartzofeldspathic mylonites and ultramylonites (Figures 9a and b). At Hare Mare Creek station 2, the disappearance of thin gouge-filled fractures coincides with a transition from micaceous-quartzofeldspathic mylonite to quartzofeldspathic mylonites (Figure 9c). Localities that showed the widest range in fracture orientations tend to be less than 160 m from the PSZs within the ultramylonites (Figure 7a). Within mylonite units, fracture orientations tend to be more aligned to the foliation (Figure 7a), although gouge-filled fractures can sometimes cut across it (e.g. Bullock Creek, Figure 7b).

4.3 Fractures in AHP drill-core, 500-1400 m from the Alpine Fault

The AHP sampled grey, well-foliated schist bedrock of the Haast Schist Group (textural zone III-IV, Turnbull et al., 2001). Foliation is defined by alternating quartzo-feldspathic and micaceous layers (Figure 10a and b). All 239 fractures measured in the CT scans of drill-core are plotted in Figure 11. There is a strong alignment of fractures to the host rock schistosity and the regional Alpine Fault orientation, in agreement with the findings during initial drill-core descriptions (Geotech Consulting Limited, 2006; Savage, 2013). Fractures that cut across

Solid Earth Discuss., https://doi.org/10.5194/se-2017-112
Manuscript under review for journal Solid Earth
Discussion started: 10 October 2017

the schistosity are most frequent in BH4 (Figure 10d and 11). Though fractures are predominantly open, it is conceivable that the original fill may have been lost during the subsequent core handling processes. This means that standard schemes to differentiate between natural and induced fractures (Kulander et al., 1990) cannot be applied to this dataset.

5 Discussion

5.1 Fracture orientations in anisotropic wall rocks in the Alpine Fault hanging-wall

Two styles of fracturing are evident in the mechanically anisotropic Alpine Fault cataclasite, mylonite and schist sequence. Within DFDP-1 core, fractures are predominantly gouge-filled and exhibit a range of orientations (Figure 5 and 6) with only a small proportion (11%) of fractures in foliated cataclasites and ultramylonites clearly foliation-parallel (Williams et al., 2016). However, in host rock schists sampled by the AHP drill-core, the fractures are predominantly foliation-parallel (Figure 11). In field transects, open, foliation-parallel fractures are found at all localities, but they are most common at distances greater than 160 m from the Alpine Fault in the mylonite and protomylonite sequence (Figure 7). Overall, there is a transition from dominantly open, foliation-parallel fractures at distances greater than 160 m from the PSZs, to gouge-filled fractures with more variable orientations closer to the fault (Figure 12).

Experimental studies on foliated rocks demonstrate that mechanical anisotropy will exert the greatest control on rock failure when: (1) the angle between σ_1 and the anisotropy (α) is ~30º, (2) confining pressure is low (<35 MPa), and (3) the mechanical 'strength' of the anisotropy is high (Donath, 1961; Misra et al., 2015; Nasseri et al., 2003; Paterson and Wong, 2005). The first factor can be approximated for the Alpine Fault given the mylonite's average orientation of 055/45SE (Norris and Cooper, 2007) and stress tensor orientation within the surrounding crust, determined from focal mechanisms of microseismicity in the Alpine Fault's hanging-wall (Boese et al., 2012). This yields a value of α of approximately 44º, when measured in the plane containing the maximum and minimum principal stresses (σ_1 and σ_3).This can be considered an intermediate value of α, since in deformation experiments fractures may form parallel or non-parallel to the foliation depending on the combination of confining pressure and lithology (Donath, 1961; Nasseri et al., 2003; Paterson and Wong, 2005).

Foliation-parallel fractures are generally least common in the ultramylonites and foliated cataclasites. Lithology may control mechanical anisotropy depending on mineralogy, porosity, grain size, and the nature of the foliation surfaces (Donath, 1961; Nasseri et al., 2003). It is notable that phase mixing and grain size reduction in the ultramylonites (Figure 2a) reduces the intensity of the foliation, compared to the relatively coarse-grained schists, protomylonites, and mylonites (Figure 2b) (Norris and Cooper, 2007; Toy et al., 2010, 2008). This data suggest this lithological change could have a marked effect on the orientation of fracturing. Compositional variations between relatively quartzofeldspathic and relatively micaceous mylonites can also influence the density of foliation-parallel fractures in some cases (Figure 9). For example, at Hare Mare Creek, there is a sharp lithological boundary between micaceous and quartzofeldspathic mylonite, and gouge-filled fractures predominate in the former, while open foliation-parallel fractures predominate in the latter (Figure 9c). These observations highlight that fracturing in the upper crust may be influenced by lithological variations imposed by an underlying linked, and synkinematic, shear zone.

However, at other localities (e.g. Stony Creek, Figure 7), variations in dominant fracture characteristics are confined within units of similar composition and texture. This indicates that variations in confining pressure are also important, with foliation-parallel fractures forming at relatively low confining pressures compared to fractures adjacent to the Alpine

Fault in the ultramylonites. Indeed, it is likely foliation-parallel fractures formed as confining pressure was released (Engelder, 1985; Price, 1959; Zangerl et al., 2006) during rapid exhumation (6-9 mm/yr) of the hanging-wall along the Alpine Fault (Little et al., 2005; Tippett and Kamp, 1995).

5.2 Fracture damage around the Alpine Fault

Caine et al., (1996) defined a fault damage zone as "a network of subsidiary structures that bound the fault core and may enhance fault zone permeability relative to the core and undeformed protolith." In applying this definition, most previous work has defined the damage zone as a volume of rock that shows elevated fracture densities compared to a "background" level of fracturing that normally includes widely-spaced regional fracture or joint sets (e.g. Berg and Skar, 2005; Faulkner et al., 2010; Savage and Brodsky, 2011; Schulz and Evans, 2000). Our data from the field transects of the Alpine Fault show that fracture density remains roughly constant (>3.5 fractures/m) for at least 500 m into the hanging-wall (Figure 7a). Furthermore, at distances 200-1500 m from the Alpine Fault an active hydrogeological system was sampled by the DFDP-2B borehole (Sutherland et al., 2017; Townend et al., 2015). Permeability in this rock mass is controlled by open fractures (Cox et al., 2015; Sutherland et al., 2017) that are foliation-parallel (Massiot, 2017), and so directly analogous to the fractures sampled in the field (Figure 8g-i) and in AHP drill-core (Figure 10).

Despite these observations, we suggest that the damage zone surrounding the Alpine Fault is most appropriately represented by the localised zone with intensive (>1 fracture/metre) broadly oriented gouge-filled fractures observed in DFDP-1 drill-core (Figures 5 and 6) and field transects (Figure 7 and 8). Microstructural and compositional analysis of these fractures indicates that they form in response to wear and shear of the surrounding of the wall rock along with silicate mineralisation from hydrothermal fluids (Warr and Cox, 2001; Williams et al., 2017a). They are considered necessary to the development of near-surface (<4 km) fault wedges that facilitate complex oblique-slip Alpine Fault movement (Barth et al., 2012; Norris and Cooper, 1997). They may also reflect the dynamic off-fault stresses associated with M_W >7.5 Alpine Fault earthquake ruptures (Sutherland et al., 2007), when the hanging-wall is in compression assuming up-dip rupture propagation (Ma and Beroza, 2008; Rice et al., 2005).

Gouge-filled fractures are present at all distances in our field transects (Figure 7-9) and within the AHP drill-core (Figure 10c). However, their interval of high density (>1 fracture/metre) is restricted to less than 118-146 m from the PSZs at Gaunt Creek (i.e. between stations 3-4), <73-103 m at Stony Creek (i.e. between stations 2-3), <151 m at Hare Mare Creek (at station 2, Figure 8c) and <155-160 m at Havelock Creek (i.e. between stations 3-4). This is consistent with the observations of Norris and Cooper, (2007) who suggested that the Alpine Fault's central section damage zone can be defined by a ~100 m wide zone of intensive gouge-filled fractures. These estimates of damage zone width are also similar to those made elsewhere on the Alpine Fault (e.g. Barth et al., 2013 in the southern section in South Westland; Wright, 1998 at the northern end of the the central section, Figure 13a) and to other predictions for crustal-scale (Figure 13b), rapidly-moving (~few cm/yr) fault zones that have accommodated hundreds of kilometres of displacement (Biegel and Sammis, 2004; Childs et al., 2009; Finzi et al., 2009; Manighetti et al., 2007; Perrin et al., 2016; Savage and Brodsky, 2011; Savage and Cooke, 2010).

5.3 Comparison to geophysical data

A relatively narrow (<100-160 m) hanging-wall damage zone is also broadly consistent with the presence of a 60-200 m wide Low Velocity Zone around the Alpine Fault, which extends to depths of 8 km (Eccles et al., 2015). This was detected by Fault Zone Guided Waves

(FZGWs) that are commonly regarded as an *in situ* indicator of fault damage (e.g. Ben-Zion and Sammis, 2003; Eberhart-Phillips et al., 1995; Ellsworth and Malin, 2011; Li et al., 2014). If the FZGWs are sampling the zone of intensive gouge-filled fracturing, it therefore indicates that the >500 m wide interval of open foliation-parallel fractures are a near-surface feature only. This is consistent with our interpretation that these fractures formed at low confining pressures during exhumation within the Alpine Fault's hanging wall.

FZGWs are a measure of total fault zone width. Since our hanging-wall damage zone width measurements are towards the higher end of the Alpine Fault FZGW estimates, much of the damage may be concentrated in the Alpine Fault's hanging wall. This is consistent with other dipping thrust faults (Li et al., 2013; Ma, 2009; Yeh et al., 2007). However, Western Province basement rocks to the west of the Alpine Fault are rarely exposed (Lund Snee et al., 2014; Norris and Cooper, 2007), so it is not possible to examine Alpine Fault footwall damage to confirm this.

Pervasive minor faults have been mapped for distances of tens of kilometres from the Alpine Fault (Cox and Barrell, 2007; Cox and Sutherland, 2007). We interpret that the occasional gouge-filled fractures observed here at distances greater than 160 m from the Alpine Fault (e.g. Figure 8e) are equivalent to this set. These fractures may also be the exhumed equivalent of structures that are currently accommodating the diffuse, low-moderate magnitude (M_W <6) seismicity that has been recorded at depths less than 10 km in the Alpine Fault's hanging-wall (Boese et al., 2012; Chamberlain et al., 2017; Eberhart‐Phillips, 1995).

6. Conclusions

Fracture orientations and densities in the foliated hanging-wall of the Alpine Fault's central section were quantified in drill-core from the Deep Fault Drilling Project (DFDP-1), field transects in four creek sections and drill-core recovered from the Amethyst Hydro Project. At distances greater than approximately 160 m from the Alpine Fault principal slip zones (PSZs), open and foliation-parallel fractures dominate. These are interpreted to form at low confining pressures in Alpine Schists and Alpine Fault mylonites that are mechanically anisotropic. At distances less than c. 160 m from the PSZs, gouge-filled fractures with a wide range of orientations predominate. Fracture density and orientation are locally influenced by changes in host rock lithology, but overall fracture density is approximately constant at distances of up to c. 500 m from the PSZs. We conclude that the Alpine Fault's hanging-wall "damage zone" is most suitably defined by the approximately 160 m-wide zone of gouge-filled fractures. These fractures formed at relatively high confining pressures and/or in relatively mechanically isotropic ultramylonites and foliated cataclasites. They are interpreted to have been generated during the development of fault wedges and/or the dynamic effect of ruptures propagating along the Alpine Fault. Comparison of our field-based estimates of damage zone width (160 m) to the total thickness of the low-velocity zone measured in geophysical data (60-200 m) suggests that the Alpine Fault damage zone is asymmetric, with most brittle fault-related damage focussed in its hanging-wall.

Code availability

The code to generate 'unrolled' circumferential CT images is available from the GFZ data service (http://pmd.gfz-potsdam.de/panmetaworks/review/7f1b114f11b67f540bb1360ead692dc578a66e3d0935c7fef6ffe210db285300-icdp/).

Data availability

In the supplementary information, we include detailed field maps and cross sections (Figure S1), a cross section through the Amethyst Tunnel and location of boreholes (Figure S2), an example of AHP CT scans (Figure S3), a list of rotations applied to DFDP-1B core (Table

Solid Earth Discuss., https://doi.org/10.5194/se-2017-112
Manuscript under review for journal Solid Earth
Discussion started: 10 October 2017

Solid Earth Discussions

S1), and a summary of field transects (Table S2). Lithological distribution and Alpine Fault location as per University of Otago fault zone mapping program, which is available at: http://www.otago.ac.nz/geology/research/structural-geology/alpine-fault/af-maps.html. DFDP-1 and AHP CT scan 'core logs' and CT-BHTV image comparison are available on the GFZ data service (http://pmd.gfz-potsdam.de/panmetaworks/review/52b75045a30f1bd60f7fd5b841e69c468885e2a10dfc3704e50b236df2ef8608-icdp).

Acknowledgements

DFDP-1 was funded by: GNS Science; Victoria University of Wellington; the University of Otago; the University of Auckland; the University of Canterbury; Deutsche Forschungsgemeinschaft and the University of Bremen; Natural Environment Research Council grants NE/J024449/1, NE/ G524160/1 and NE/H012486/1 and the University of Liverpool; and the Marsden Fund of the Royal Society of New Zealand. The International Continental Scientific Drilling Program, ICDP (www.icdp-online.org) provided extensive support. JW was supported by a University of Otago Doctoral Scholarship. We thank Darren Tod at the Southern Cross Hospital, Wellington, for support in collecting CT scans of Amethyst Hydro Project Core. Katrina Sauer, Ben Melosh and Astrid Vetrhus provided field assistance. Comments by two anonymous reviewers in an earlier version of this manuscript improved this paper.

Appendix A: DFDP-1B core rotation methodology

The technique employed to reorient core DFDP-1 here is similar to that described in Jarrard et al., (2001), Paulsen et al., (2002) and Shigematsu et al., (2014), however, instead of comparing DFDP-1 BHTV data to DMT CoreScan system® unrolled core scans, we compare BTHV images to 'unrolled' CT core images. The acquisition and interpretation of the DFDP-

1 BHTV logs has been previously described by Townend et al., (2013) and McNamara, (2015). DFDP-1 CT scans consist of a stack of core-axial perpendicular image slices with a pixel size of 0.244 mm and a spacing of 1 mm. The CT stack for each core section was loaded into Fiji (http://fiji.sc/Fiji) and a circle was manually defined around the irregular boundary of drill-core in a core axial-perpendicular image slice using the code available at Mills and Williams, (2017). This circle was then used to define the path of the image in all other slices. Generation of the unrolled images accounts for the fact that the spacing between individual CT slices (1 mm, i.e. the core-axial parallel pixel size) is greater than the pixel size within the slices (0.244 mm). Unrolled images were then reflected around the borehole axis as an image of the outer surface of the core and a BHTV image are reflections of each other. This technique has benefits over methods using the DMT CoreScan system®, since drill-core does not have to be physically rotated and so can be used without the risk of damaging fragile core sections.

Unrolled CT images were imported into the composite log viewing software WellCAD® (http://www.alt.lu/wellcad.htm) along with the BHTV images, where they are placed side-by-side to allow matching of structures (Figure 4, see also Williams et al., (2017b)). When correlating the two datasets, it was first necessary to account for possible depth shifts between recorded drill-core depths and BHTV imagery due to factors such as stretching of the logging cable and intervals from which no drill-core was recovered (Haggas et al., 2001; Jarrard et al., 2001). In this study, depth shifts of no more than ±30 cm were allowed.

The orientation of fractures in the DFDP-1 CT images had previously been measured within a local core reference frame (see Figure 4 in Williams et al., 2016). Since the DFDP-1 boreholes were vertical, corrections to reorient the drill-core back into a geographic reference frame required only a single rotation about the core axis to correct for the dip direction. When correlating structures, errors may be introduced by: (1) the internal BHTV magnetometer

(±2°), (2) the manual picking of sinusoidal curves on BHTV and unrolled CT images that can be ±10° for shallowly dipping (<30°) structures (Jarrard et al., 2001), and (3) the fact that the DFDP-1B BHTV data imaged the open borehole, which has a larger diameter (127 mm) than the drill-core (85 mm). To mitigate against the cumulative effect of these errors, Jarrard et al., (2001) stitched unrolled images of many different core sections together that spanned intervals of 5-30 m, prior to the matching with BHTV imagery. This meant that only a single rotation was necessary for all core sections across the entire stitched interval, which could be based on identifying ~20-30 matching structures between the BHTV and unrolled core images.

In DFDP-1 it was not possible to stitch unrolled CT images of core section together as no prominent reference marker across different sections were identified. Consequently each <1 m long core section had to be reoriented individually, within which we never identified more than 3 matching structures. Therefore, compared to the methodology described by Jarrard et al., (2001), the degree of confidence on the applied reorientation was strongly dependent on the quality of individual matches for each core section and the range of rotations that they indicated. We recorded this qualitatively for each core section using the scheme outlined below.

- High degree of confidence: images matched with one very prominent structure (e.g. Figure 4d), or matched with two or more structures whose range of suggested rotations are within 10° of each other (Figure 4b and c).

- Moderate degree of confidence: images matched with one prominent feature or two features that indicate rotations that range 10-19° (e.g. Figure 4a) or three features whose range of suggested rotations are within 20-30° of each other.

Solid Earth Discuss., https://doi.org/10.5194/se-2017-112
Manuscript under review for journal Solid Earth
Discussion started: 10 October 2017

Solid Earth Discussions

- Low degree of confidence: images matched with one feature or two features whose range of suggested rotations are within 20-30° of each other.

In this scheme, a core reorientation is deemed unreliable if the range of rotations suggested by different structures is ≥30°, i.e. equivalent to the cumulative effect of possible errors listed above. For those core sections where more than one matching structure was identified, the rotation that was applied was derived from the average of that required for each match. If one of the matched structures was more prominent, then the applied rotation was biased towards that structure.

Appendix B: DFDP-1B core rotation validity

Based on the criteria presented in Appendix A, of the 40 core sections from DFDP-1B in which there was suitable quality of unrolled CT and BHTV images to attempt reorientation (Figure 3), 31 were reoriented (Table S1). Prior to reorientation, fractures in these sections exhibit no clustering (Figure A1a), however, a weak one does develop after reorientation (Figure 5a). Since fractures in nature typically exhibit non-random orientations, this is evidence that the reorientation of the CT scans was successful (Kulander et al., 1990; Paulsen et al., 2002). In addition, fractures within some individual core sections (Figure A1b), and fractures rotated based on a high degree of confidence (Figure A1c) contain a wide range of orientations.

The recognition of fractures in unrolled CT images that are not observed in BHTV can be readily explained by the higher resolution of the CT images. However, structures are also observed in the BHTV logs, but not interpreted as fractures in the CT images (Figure 4). This may represent noise in the BHTV images, or in the case of foliation-parallel structures, the ultramylonitic foliation itself since it can be difficult to differentiate these structures. The subordinate north-dipping set of fractures in the BHTV images (Figure 5b) is not recognised in the orientations gathered from CT images (Figure 5a). A similar north dipping fracture set was also recognised in DFDP-2B BHTV images (Massiot 2017), and their causation and relevance is the focus of ongoing work.

Competing Interests

Authors declare that they have no conflict of interest.

References

Allen, M. J., Tatham, D., Faulkner, D. R., Mariani, E. and Boulton, C.: Permeability and seismic velocity and their anisotropy across the Alpine Fault, New Zealand: An insight from laboratory measurements on core from the Deep Fault Drilling Project phase 1 (DFDP-1), J. Geophys. Res. Solid Earth, 122(8), 6160–6179, doi:10.1002/2017JB014355, 2017.

Andrews, D. J.: Rupture dynamics with energy loss outside the slip zone, J. Geophys. Res. Solid Earth, 110(1), 1–14, doi:10.1029/2004JB003191, 2005.

Barth, N. C., Toy, V. G., Langridge, R. M. and Norris, R. J.: Scale dependence of oblique plate-boundary partitioning: New insights from LiDAR, central Alpine fault, New Zealand, Lithosphere, 4(5), 435–448, doi:10.1130/L201.1, 2012.

Barth, N. C., Boulton, C., Carpenter, B. M., Batt, G. E. and Toy, V. G.: Slip localization on the southern Alpine Fault New Zealand, Tectonics, 32(3), 620–640, doi:10.1002/tect.20041, 2013.

Ben-Zion, Y. and Sammis, C. G.: Characterization of Fault Zones, Pure Appl. Geophys., 160(3), 677–715, doi:10.1007/PL00012554, 2003.

Berg, S. S. and Skar, T.: Controls on damage zone asymmetry of a normal fault zone: Outcrop analyses of a segment of the Moab fault, SE Utah, J. Struct. Geol., 27(10), 1803–1822, doi:10.1016/j.jsg.2005.04.012, 2005.

Biegel, R. L. and Sammis, C. G.: Relating Fault Mechanics to Fault Zone Structure, Adv.

Geophys., 47(C), 65–111, doi:10.1016/S0065-2687(04)47002-2, 2004.

Bistacchi, A., Massironi, M. and Menegon, L.: Three-dimensional characterization of a crustal-scale fault zone: The Pusteria and Sprechenstein fault system (Eastern Alps), J. Struct. Geol., 32(12), 2022–2041, doi:10.1016/j.jsg.2010.06.003, 2010.

Bistacchi, A., Massironi, M., Menegon, L., Bolognesi, F. and Donghi, V.: On the nucleation of non-Andersonian faults along phyllosilicate-rich mylonite belts, Geol. Soc. London, Spec. Publ., 367(1), 185–199, doi:10.1144/sp367.13, 2012.

Boese, C. M. M., Townend, J., Smith, E. and Stern, T.: Microseismicity and stress in the vicinity of the Alpine Fault, central Southern Alps, New Zealand, J. Geophys. Res. Solid Earth, 117(2), doi:10.1029/2011JB008460, 2012.

Boulton, C., Yao, L., Faulkner, D. R., Townend, J., Toy, V. G., Sutherland, R., Ma, S. and Shimamoto, T.: High-velocity frictional properties of Alpine Fault rocks: Mechanical data, microstructural analysis, and implications for rupture propagation, J. Struct. Geol., 97, 71–92, doi:10.1016/j.jsg.2017.02.003, 2017.

Boulton, C. J., Carpenter, B. M., Toy, V. and Marone, C.: Physical properties of surface outcrop cataclastic fault rocks, Alpine Fault, New Zealand, Geochemistry, Geophys. Geosystems, 13(1), doi:10.1029/2011GC003872, 2012.

Caine, J. S., Evans, J. P. and Forster, C. B.: Fault zone architecture and permeability structure, Geology, 24(11), 1025–1028, 1996.

Chamberlain, C. J., Boese, C. M. and Townend, J.: Cross-correlation-based detection and characterisation of microseismicity adjacent to the locked, late-interseismic Alpine Fault, South Westland, New Zealand, Earth Planet. Sci. Lett., 457, 63–72, doi:10.1016/j.epsl.2016.09.061, 2017.

Chester, F. M. and Chester, J. S.: Stress and deformation along wavy frictional faults, J. Geophys. Res., 105(B10), 23421, doi:10.1029/2000JB900241, 2000.

Solid Earth Discuss., https://doi.org/10.5194/se-2017-112
Manuscript under review for journal Solid Earth
Discussion started: 10 October 2017

Chester, F. M. and Logan, J. M.: Implications for mechanical properties of brittle faults from observations of the Punchbowl fault zone, California, Pure Appl. Geophys. PAGEOPH, 124(1–2), 79–106, doi:10.1007/BF00875720, 1986.

Chester, F. M., Evans, J. P. and Biegel, R. L.: Internal structure and weakening mechanisms of the San Andreas Fault, J. Geophys. Res., 98(B1), 771, doi:10.1029/92JB01866, 1993.

Chester, J. S. and Fletcher, R. C.: Stress distribution and failure in anisotropic rock near a bend on a weak fault, J. Geophys. Res. Earth, 102(B1), 693–708, doi:10.1029/96JB02791, 1997.

Childs, C., Manzocchi, T., Walsh, J. J., Bonson, C. G., Nicol, A. and Schöpfer, M. P. J.: A geometric model of fault zone and fault rock thickness variations, J. Struct. Geol., 31(2), 117–127, doi:10.1016/j.jsg.2008.08.009, 2009.

Choi, J. H., Edwards, P., Ko, K. and Kim, Y. S.: Definition and classification of fault damage zones: A review and a new methodological approach, Earth-Science Rev., 152, 70–87, doi:10.1016/j.earscirev.2015.11.006, 2016.

Cochran, E. S., Li, Y. G., Shearer, P. M., Barbot, S., Fialko, Y. and Vidale, J. E.: Seismic and geodetic evidence for extensive, long-lived fault damage zones, Geology, 37(4), 315–318, doi:10.1130/G25306A.1, 2009.

Cooper, A. F. and Norris, R. J.: Anatomy, structural evolution, and slip rate of a plate-boundary thrust: the Alpine Fault at Gaunt Creek, Westland, New Zealand, Geol. Soc. Am. Bull., 106(5), 627–633, doi:10.1130/0016-7606(1994)106<0627:ASEASR>2.3.CO;2, 1994.

Cooper, A. F. and Norris, R. J.: Inverted metamorphic sequences in Alpine fault mylonites produced by oblique shear within a plate boundary fault zone, New Zealand., 2011.

Cowie, P. A. and Scholz, C. H.: Physical Explanation for the Displacement Length Relationship of Faults Using a Post-Yield Fracture-Mechanics Model, J. Struct. Geol., 14(10), 1133–1148, doi:10.1016/0191-8141(92)90065-5, 1992.

Cox, S. C. and Barrell, D. J. A.: Geology of the Aoraki area, Institute of Geological & Nuclear Sciences., 2007.

Cox, S. C. and Sutherland, R.: Regional Geological Framework of South Island, New Zealand, and its Significance for Understanding the Active Plate Boundary, A Cont. Plate Bound. Tectonics South Island, New Zeal., 175, 19–46, doi:10.1029/175GM03, 2007.

Cox, S. C., Menzies, C. D., Sutherland, R., Denys, P. H., Chamberlain, C. and Teagle, D. A. H.: Changes in hot spring temperature and hydrogeology of the Alpine Fault hanging wall, New Zealand, induced by distal South Island earthquakes, Geofluids, 15(1–2), 216–239, 2015.

DeMets, C., Gordon, R. G., Argus, D. F. and Stein, S.: Effect of recent revisions to the geomagnetic reversal time scale on estimate of current plate motions, Geophys. Res. Lett., 21(20), 2191–2194, doi:10.1029/94GL02118, 1994.

Donath, F. A.: Experimental study of shear failure in anisotropic rocks, Geol. Soc. Am. Bull., 72(6), 985–989, doi:10.1130/0016-7606(1961)72[985:ESOSFI]2.0.CO;2, 1961.

Eberhart-Phillips, D., Stanley, W. D., Rodriguez, B. D. and Lutter, W. J.: Surface seismic and electrical methods to detect fluids related to faulting, J. Geophys. Res., 100(B7), 12919–12936, doi:10.1029/94JB03256, 1995.

Eberhart-Phillips, D.: Examination of seismicity in the central Alpine fault region, South Island, New Zealand, New Zeal. J. Geol. Geophys., 38(4), 571–578, 1995.

Eccles, J. D., Gulley, A. K., Malin, P. E., Boese, C. M., Townend, J. and Sutherland, R.: Fault Zone Guided Wave generation on the locked, late interseismic Alpine Fault, New Zealand, Geophys. Res. Lett., 42(14), 5736–5743, doi:10.1002/2015GL064208, 2015.

Ellsworth, W. L. and Malin, P. E.: Deep rock damage in the San Andreas Fault revealed by P- and S-type fault-zone-guided waves, Fagereng, A., Toy, V.G., Rowland, J. (Eds), Geol. Earthq. Source A Vol. Honor Rick Sibson, Geol. Soc. London, Spec. Publ., 359(1), 39–53, doi:10.1144/SP359.3, 2011.

Engelder, T.: Loading paths to joint propagation during a tectonic cycle: an example from the Appalachian Plateau, U.S.A., J. Struct. Geol., 7(3–4), 459–476, doi:10.1016/0191-8141(85)90049-5, 1985.

Faulkner, D. R., Jackson, C. A. L., Lunn, R. J., Schlische, R. W., Shipton, Z. K., Wibberley, C. A. J. and Withjack, M. O.: A review of recent developments concerning the structure, mechanics and fluid flow properties of fault zones, J. Struct. Geol., 32(11), 1557–1575, doi:10.1016/j.jsg.2010.06.009, 2010.

Faulkner, D. R., Mitchell, T. M., Jensen, E. and Cembrano, J.: Scaling of fault damage zones with displacement and the implications for fault growth processes, J. Geophys. Res. Solid Earth, 116(5), doi:10.1029/2010JB007788, 2011.

Finzi, Y., Hearn, E. H., Ben-Zion, Y. and Lyakhovsky, V.: Structural properties and deformation patterns of evolving strike-slip faults: Numerical simulations incorporating damage rheology, Pure Appl. Geophys., 166(10–11), 1537–1573, doi:10.1007/s00024-009-0522-1, 2009.

Geotech Consulting Limited: Amethyst Hydro Scheme Drilling Investigation Summary Report., 2006.

Haggas, S., Brewer, T. S., Harvey, P. K. and Iturrino, G. I.: Relocating and orientating cores by the integration of electrical and optical images, J. Geol. Soc. London, 158, 615–623, doi:10.1144/jgs.158.4.615, 2001.

Hudson, J. A.: Discontinuity Frequency in Rock Masses - Hudson e Priest 1983.pdf, in International Journal of Rock Mechanics and Mining Sciences & Geomechanics Abstracts, vol. 20, pp. 73–89, Elsevier., 1983.

Ikari, M. J., Carpenter, B. M., Kopf, A. J. and Marone, C.: Frictional strength, rate-dependence, and healing in DFDP-1 borehole samples from the Alpine Fault, New Zealand, Tectonophysics, 630(C), 1–8, doi:10.1016/j.tecto.2014.05.005, 2014.

Jarrard, R. D., Paulsen, T. S. and Wilson, T. J.: Orientation of CRP-3 core, Victoria Land

Basin, Antarctica, Terra Antarct., 8(3), 161–166, 2001.

Kim, Y. S. and Sanderson, D. J.: Fault propagation, displacement and damage zones, Struct. Geol. New Res., 1, 99–117, 2008.

Kim, Y. S., Peacock, D. C. P. and Sanderson, D. J.: Fault damage zones, J. Struct. Geol., 26(3), 503–517, doi:10.1016/j.jsg.2003.08.002, 2004.

Kulander, B. R., Dean, S. L. and Ward, B. J.: Fracture core analysis: interpretation, logging and use of natural and induced fractures in core, American Association of Petroleum Geologists., 1990.

Lees, J. M.: RFOC: Graphics for spherical distributions and earthquake focal mechanisms. R package version 3.3-3. http://CRAN.R-project.org/package=RFOC, R Packag. version, 3(2), 2014.

Li, H., Wang, H., Xu, Z., Si, J., Pei, J., Li, T., Huang, Y., Song, S. R., Kuo, L. W., Sun, Z., Chevalier, M. L. and Liu, D.: Characteristics of the fault-related rocks, fault zones and the principal slip zone in the Wenchuan Earthquake Fault Scientific Drilling Project Hole-1 (WFSD-1), Tectonophysics, 584, 23–42, doi:10.1016/j.tecto.2012.08.021, 2013.

Li, Y. G., De Pascale, G. P., Quigley, M. C. and Gravley, D. M.: Fault damage zones of the M7.1 Darfield and M6.3 Christchurch earthquakes characterized by fault-zone trapped waves, Tectonophysics, 618, 79–101, doi:10.1016/j.tecto.2014.01.029, 2014.

Little, T. A., Cox, S., Vry, J. K. and Batt, G.: Variations in exhumation level and uplift rate along the obliqu-slip Alpine fault, central Southern Alps, New Zealand, Geol. Soc. Am. Bull., 117(5), 707, doi:10.1130/B25500.1, 2005.

Lund Snee, J. E., Toy, V. G. and Gessner, K.: Significance of brittle deformation in the footwall of the Alpine Fault, New Zealand: Smithy Creek Fault zone, J. Struct. Geol., 64, 79–98, doi:10.1016/j.jsg.2013.06.002, 2014.

Ma, S.: Distinct asymmetry in rupture-induced inelastic strain across dipping faults: An off-fault yielding model, Geophys. Res. Lett., 36(20), doi:10.1029/2009GL040666, 2009.

Ma, S. and Beroza, G. C.: Rupture dynamics on a bimaterial interface for dipping faults, Bull. Seismol. Soc. Am., 98(4), 1642–1658, doi:10.1785/0120070201, 2008.

Manighetti, I., Campillo, M., Bouley, S. and Cotton, F.: Earthquake scaling, fault segmentation, and structural maturity, Earth Planet. Sci. Lett., 253(3–4), 429–438, doi:10.1016/j.epsl.2006.11.004, 2007.

Massiot, C.: Fracture system characterisation and implications for fluid flow in volcanic and metamorphic rocks, 2017.

Massiot, C., Mcnamara, D. D. and Lewis, B.: Geothermics Processing and analysis of high temperature geothermal acoustic borehole image logs in the Taupo Volcanic Zone , New Zealand, Geothermics, 53, 190–201, doi:10.1016/j.geothermics.2014.05.010, 2015.

Massironi, M., Bistacchi, A. and Menegon, L.: Misoriented faults in exhumed metamorphic complexes: Rule or exception?, Earth Planet. Sci. Lett., 307(1–2), 233–239, doi:10.1016/j.epsl.2011.04.041, 2011.

McNamara, D.: Exploring New Zealand's subsurface using borehole images, in Presented at the 2015 New Zealand Geosciences Conference, Wellington, 25-27th November (2015)., 2015.

Mills, S. and Williams, J. N.: Generating circumferential images of tomographic drill-core scans, GFZ Data Serv., doi:http://doi.org/10.5880/ICDP.5052.005, 2017.

Misra, S., Ellis, S. and Mandal, N.: Fault damage zones in mechanically layered rocks: The effects of planar anisotropy, J. Geophys. Res. B Solid Earth, 120(8), 5432–5452, doi:10.1002/2014JB011780, 2015.

Mitchell, T. M. and Faulkner, D. R.: The nature and origin of off-fault damage surrounding strike-slip fault zones with a wide range of displacements: A field study from the Atacama fault system, northern Chile, J. Struct. Geol., 31(8), 802–816, doi:10.1016/j.jsg.2009.05.002,

Solid Earth Discuss., https://doi.org/10.5194/se-2017-112
Manuscript under review for journal Solid Earth
Discussion started: 10 October 2017

2009.

Mitchell, T. M. and Toy, V. G.: Photograph of the month, J. Struct. Geol., 61, 143, doi:10.1016/j.jsg.2014.01.004, 2014.

Muir-Wood, R. and King, G. C. P.: Hydrological signatures of earthquake strain, J. Geophys. Res., 98(B12), 22035, doi:10.1029/93JB02219, 1993.

Nasseri, M. H. B., Rao, K. S. and Ramamurthy, T.: Anisotropic strength and deformation behavior of Himalayan schists, Int. J. Rock Mech. Min. Sci., 40(1), 3–23, doi:10.1016/S1365-1609(02)00103-X, 2003.

Norris, R. J. and Cooper, A. F.: Origin of small-scale segmentation and transpressional thrusting along the Alpine Fault, New Zealand, Geol. Soc. Am. Bull., 107(2), 231–240, doi:10.1130/0016-7606(1995)107<0231:OOSSSA>2.3.CO;2, 1995.

Norris, R. J. and Cooper, A. F.: Erosional control on the structural evolution of a transpressional thrust complex on the Alpine fault, New Zealand, J. Struct. Geol., 19(10), 1323–1342, doi:10.1016/S0191-8141(97)00036-9, 1997.

Norris, R. J. and Cooper, A. F.: Late Quaternary slip rates and slip-partitioning on the Alpine Fault, New Zealand, J. Struct. Geol., 23(2000), 507–520, 2001.

Norris, R. J. and Cooper, A. F.: Very high strains recorded in mylonites along the Alpine Fault, New Zealand: implications for the deep structure of plate boundary faults, J. Struct. Geol., 25(12), 2141–2157, 2003.

Norris, R. J. and Cooper, A. F.: The Alpine Fault, New Zealand: Surface Geology and Field Relationships, in A Continental Plate Boundary: Tectonics at South Island, New Zealand, edited by D. Okaya, T. A. Stern, and F. Davey, pp. 157–175, American Geophysical Union., 2007.

Norris, R. J. and Toy, V. G.: Continental transforms: A view from the Alpine Fault, J. Struct. Geol., 64, 3–31, doi:10.1016/j.jsg.2014.03.003, 2014.

Solid Earth Discuss., https://doi.org/10.5194/se-2017-112
Manuscript under review for journal Solid Earth
Discussion started: 10 October 2017

O'Brien, G. A., Cox, S. C. and Townend, J.: Spatially and temporally systematic hydrologic changes within large geoengineered landslides, Cromwell Gorge, New Zealand, induced by multiple regional earthquakes, J. Geophys. Res. Solid Earth, 121(12), 8750–8773, 2016.

Paterson, M. S. and Wong, T. F.: Experimental rock deformation - The brittle field, Springer-Verlag Berlin Heidelberg., 2005.

Paulsen, T. S., Jarrard, R. D. and Wilson, T. J.: A simple method for orienting drill core by correlating features in whole-core scans and oriented borehole-wall imagery, J. Struct. Geol., 24(8), 1233–1238, doi:10.1016/S0191-8141(01)00133-X, 2002.

Peacock, D. C. P. and Sanderson, D. J.: Effects of layering and anisotropy on fault geometry, J. Geol. Soc. London., 149(5), 793–802, doi:10.1144/gsjgs.149.5.0793, 1992.

Peacock, D. C. P., Nixon, C. W., Rotevatn, A., Sanderson, D. J. and Zuluaga, L. F.: Glossary of fault and other fracture networks, J. Struct. Geol., 92, 12–29, doi:10.1016/j.jsg.2016.09.008, 2016.

Perrin, C., Manighetti, I., Ampuero, J. P., Cappa, F. and Gaudemer, Y.: Location of largest earthquake slip and fast rupture controlled by along-strike change in fault structural maturity due to fault growth, J. Geophys. Res. Solid Earth, 121(5), 3666–3685, doi:10.1002/2015JB012671, 2016.

Price, N. J.: Mechanics of jointing in rocks, Geol. Mag., 96(2), 149–167, doi:10.1017/S0016756800060040, 1959.

Rattenbury, M. and Isaac, M.: The QMAP 1:250 000 Geological Map of New Zealand project, New Zeal. J. Geol. Geophys., 8306(April), doi:10.1080/00288306.2012.725417, 2012.

Reed, J. J.: Mylonites, cataclasites, and associated rocks along the Alpine fault, South Island, New Zealand, New Zeal. J. Geol. Geophys., 7(4), 645–684, doi:10.1080/00288306.1964.10428124, 1964.

Rice, J. R., Sammis, C. G. and Parsons, R.: Off-fault secondary failure induced by a dynamic slip pulse, Bull. Seismol. Soc. Am., 95(1), 109–134, doi:10.1785/0120030166, 2005.

Savage, E.: Investigating Rock Mass Conditions and Implications for Tunnelling and Construction of the Amethyst Hydro Project, Harihari, University of Canterbury., 2013.

Savage, H. M. and Brodsky, E. E.: Collateral damage: Evolution with displacement of fracture distribution and secondary fault strands in fault damage zones, J. Geophys. Res. Solid Earth, 116(3), doi:10.1029/2010JB007665, 2011.

Savage, H. M. and Cooke, M. L.: Unlocking the effects of friction on fault damage zones, J. Struct. Geol., 32(11), 1732–1741, doi:10.1016/j.jsg.2009.08.014, 2010.

Savage, H. M., Keranen, K. M., Schaff, D. and Dieck, C.: Possible Precursory Signals in Damage Zone Foreshocks, Geophys. Res. Lett., 2017.

Schulz, S. E. and Evans, J. P.: Mesoscopic structure of the Punchbowl Fault, Southern California and the geologic and geophysical structure of active strike-slip faults, J. Struct. Geol., 22(7), 913–930, doi:10.1016/S0191-8141(00)00019-5, 2000.

Shigematsu, N., Otsubo, M., Fujimoto, K. and Tanaka, N.: Orienting drill core using borehole-wall image correlation analysis, J. Struct. Geol., 67(PB), 293–299, doi:10.1016/j.jsg.2014.01.016, 2014.

Sibson, R. H.: Earthquake faulting as a structural process, J. Struct. Geol., 11(1–2), 1–14, doi:10.1016/0191-8141(89)90032-1, 1989.

Sibson, R. H., White, S. H. and Atkinson, B. K.: Structure and distribution of fault rocks in the Alpine Fault Zone, New Zealand, Geol. Soc. London, Spec. Publ., 9(1), 197–210, 1981.

Simpson, G. D. H., Cooper, A. F. and Norris, R. J.: Late Quaternary evolution of the Alpine Fault Zone at Paringa, South Westland, New Zealand, New Zeal. J. Geol. Geophys., 37(1), 49–58, doi:10.1080/00288306.1994.9514600, 1994.

Stanley, C. R. and Hooper, J. J.: POND: An Excel spreadsheet to obtain structural attitudes of planes from oriented drillcore, Comput. Geosci., 29(4), 531–537, doi:10.1016/S0098-3004(03)00033-5, 2003.

Stern, T., Okaya, D., Kleffmann, S., Scherwath, M., Henrys, S. and Davey, F.: Geophysical exploration and dynamics of the Alpine Fault Zone, A Cont. Plate Bound. Tectonics South Island, New Zeal. Geophys. Monogr. Ser. 175, 207–233, doi:10.1029/175GM11, 2007.

Sutherland, R., Eberhart-Phillips, D., Harris, R. A., Stern, T., Beavan, J., Ellis, S., Henrys, S., Cox, S., Norris, R. J., Berryman, K. R., Townend, J., Bannister, S., Pettinga, J., Leitner, B., Wallace, L., Little, T. A., Cooper, A. F., Yetton, M. and Stirling, M.: Do Great Earthquakes Occur on the Alpine Fault in Central South Island, New Zealand?, in A Continental Plate Boundary: Tectonics at South Island, New Zealand, vol. 175, edited by D. Okaya, Stern, T., and F. Davey, pp. 235–251, American Geophysical Union., 2007.

Sutherland, R., Toy, V. G., Townend, J., Cox, S. C., Eccles, J. D., Faulkner, D. R., Prior, D. J., Norris, R. J., Mariani, E., Boulton, C., Carpenter, B. M., Menzies, C. D., Little, T. A., Hasting, M., De Pascale, G. P., Langridge, R. M., Scott, H. R., Reid Lindroos, Z., Fleming, B. and Kopf, J.: Drilling reveals fluid control on architecture and rupture of the Alpine fault, New Zealand, Geology, 40(12), 1143–1146, doi:10.1130/G33614.1, 2012.

Sutherland, R., Townend, J., Toy, V. G., Upton, P., Coussens, J. and DFDP2, S. T.: Extreme hydrothermal conditions at an active plate-bounding fault, Nature, 546, 137–140, doi:10.1038/nature22355, 2017.

Templeton, E. L. and Rice, J. R.: Off-fault plasticity and earthquake rupture dynamics: 2. Effects of fluid saturation, J. Geophys. Res. Solid Earth, 113(9), doi:10.1029/2007JB005530, 2008.

Terzaghi, R. D.: Sources of Error in Joint Surveys, Géotechnique, 15(3), 287–304, doi:10.1680/geot.1965.15.3.287, 1965.

Tippett, J. M. and Kamp, P. J. J.: Quantitative relationships between uplift and relief parameters for the Southern Alps, New Zealand, as determined by fission track analysis,

Solid Earth Discuss., https://doi.org/10.5194/se-2017-112
Manuscript under review for journal Solid Earth
Discussion started: 10 October 2017

Earth Surf. Process. Landforms, 20(2), 153–175, 1995.

Townend, J., Sutherland, R., Toy, V. G., Eccles, J. D., Boulton, C., Cox, S. C. and McNamara, D.: Late-interseismic state of a continental plate-bounding fault: Petrophysical results from DFDP-1 wireline logging and core analysis, Alpine Fault, New Zealand, Geochemistry, Geophys. Geosystems, 14(9), 3801–3820, doi:10.1002/ggge.20236, 2013.

Townend, J., Sutherland, R., Toy, V., Doan, M. L., Celerier, B. P., Massiot, C., Coussens, J., Capova, L. and Jeppson, T.: Petrophysical, Structural, and Hydrogeological Characteristics of the Alpine Fault Hanging Wall Based on DFDP-2 Wireline Logging, Temperature, and Hydraulic Measurements, in AGU Fall Meeting Abstracts., 2015.

Toy, V.: Rheology of the Alpine Fault mylonite zone: deformation processes at and below the base of the seismogenic zone in a major plate boundary structure, University of Otago., 2008.

Toy, V. G., Prior, D. J. and Norris, R. J.: Quartz fabrics in the Alpine Fault mylonites: Influence of pre-existing preferred orientations on fabric development during progressive uplift, J. Struct. Geol., 30(5), 602–621, doi:10.1016/j.jsg.2008.01.001, 2008.

Toy, V. G., Craw, D., Cooper, A. F. and Norris, R. J.: Thermal regime in the central Alpine Fault zone, New Zealand: Constraints from microstructures, biotite chemistry and fluid inclusion data, Tectonophysics, 485(1–4), 178–192, doi:10.1016/j.tecto.2009.12.013, 2010.

Toy, V. G., Boulton, C. J., Sutherland, R., Townend, J., Norris, R. J., Little, T. A., Prior, D. J., Mariani, E., Faulkner, D., Menzies, C. D., Scott, H. and Carpenter, B. M.: Fault rock lithologies and architecture of the central Alpine fault, New Zealand, revealed by DFDP-1 drilling, Lithosphere, 7(2), 155–173, doi:10.1130/l395.1, 2015.

Turnbull, I. M., Mortimer, N. and Craw, D.: Textural zones in the Haast Schist—a reappraisal, New Zeal. J. Geol. Geophys., 44(1), 171–183, doi:10.1080/00288306.2001.9514933, 2001.

Vermilye, J. M. and Scholz, C. H.: The process zone: A microstructural view of fault growth, J. Geophys. Res. Earth, 103(B6), 12223–12237, doi:10.1029/98JB00957, 1998.

Solid Earth Discuss., https://doi.org/10.5194/se-2017-112
Manuscript under review for journal Solid Earth
Discussion started: 10 October 2017

Warr, L. N. and Cox, S.: Clay mineral transformations and weakening mechanisms along the Alpine Fault, New Zealand, in Geological Society, London, Special Publications, vol. 186, edited by R. E. Holdsworth, R. A. Strachan, J. F. Magloughlin, and R. J. Knipe, pp. 85–101, The Geological Society, London., 2001.

Wellman, H.: Data for the Study of Recent and Late Pleistocene Faulting in the South, New Zeal. J. Sci. Technol., 34(4), 270–288, 1953.

Williams, J. N., Toy, V. G., Massiot, C., McNamara, D. D. and Wang, T.: Damaged beyond repair? Characterising the damage zone of a fault late in its interseismic cycle, the Alpine Fault, New Zealand, J. Struct. Geol., 90, 76–94, doi:10.1016/j.jsg.2016.07.006, 2016.

Williams, J. N., Toy, V. G., Smith, S. A. F. and Boulton, C.: Fracturing, fluid-rock interaction and mineralisation during the seismic cycle along the Alpine Fault, J. Struct. Geol., 103, 151–166, doi:https://doi.org/10.1016/j.jsg.2017.09.011, 2017a.

Williams, J. N., Toy, V. G., Massiot, C. and McNamara, D.: X-ray Computed Tomography and borehole televiewer images of the Alpine Fault's hanging-wall, New Zealand: Deep Fault Drilling Project phase 1 (DFDP-1) and Amethyst Hydro Project (AHP), GFZ Data Serv., doi:http://doi.org/10.5880/ICDP.5052.004, 2017b.

Wilson, J. E., Chester, J. S. and Chester, F. M.: Microfracture analysis of fault growth and wear processes, Punchbowl Fault, San Andreas system, California, J. Struct. Geol., 25(11), 1855–1873, doi:10.1016/S0191-8141(03)00036-1, 2003.

Wright, C. A.: Geology and paleoseismicity of the central Alpine Fault, New Zealand., 1998.

Yeh, E. C., Sone, H., Nakaya, T., Ian, K. H., Song, S. R., Hung, J. H., Lin, W., Hirono, T., Wang, C. Y., Ma, K. F., Soh, W. and Kinoshita, M.: Core description and characteristics of fault zones from Hole-A of the Taiwan Chelungpu-Fault Drilling Project, Terr. Atmos. Ocean. Sci., 18(2), 327–357, doi:10.3319/TAO.2007.18.2.327(TCDP), 2007.

Yukutake, Y., Ito, H., Honda, R., Harada, M., Tanada, T. and Yoshida, A.: Fluid-induced swarm earthquake sequence revealed by precisely determined hypocenters and focal

Solid Earth Discuss., https://doi.org/10.5194/se-2017-112
Manuscript under review for journal Solid Earth
Discussion started: 10 October 2017

Solid Earth Discussions

mechanisms in the 2009 activity at Hakone volcano, Japan, J. Geophys. Res. Solid Earth, 116(4), doi:10.1029/2010JB008036, 2011.

Zangerl, C., Loew, S. and Eberhardt, E.: Structure, geometry and formation of brittle discontinuities in anisotropic crystalline rocks of the central Gotthard massif, Switzerland, Eclogae Geol. Helv., 99(2), 271–290, doi:10.1007/s00015-006-1190-0, 2006.

Solid Earth Discuss., https://doi.org/10.5194/se-2017-112
Manuscript under review for journal Solid Earth
Discussion started: 10 October 2017

List of Figures

Figure 1

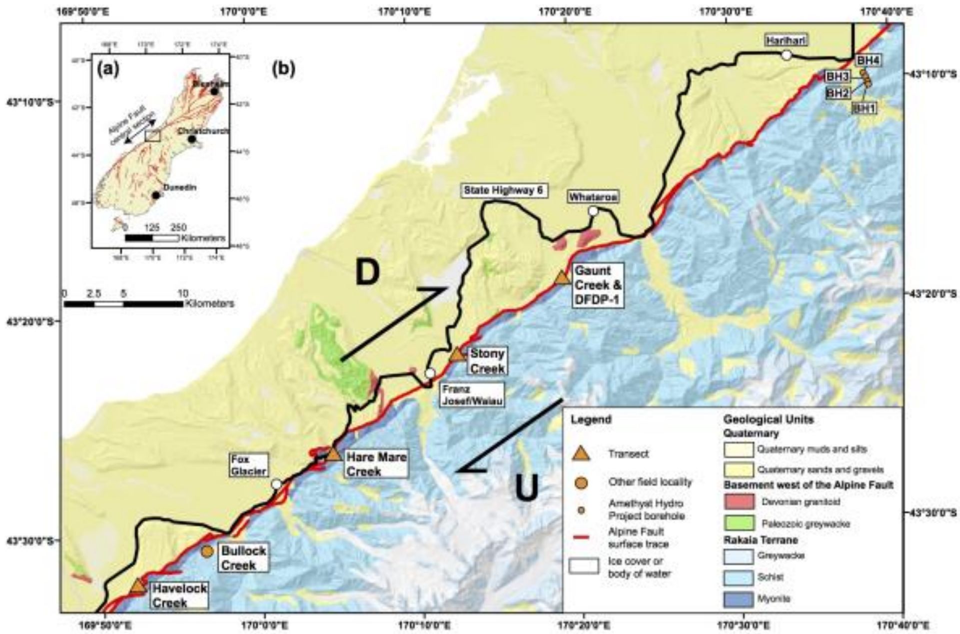

Figure 1: (a) Location map for Alpine Fault and all other onshore active faults on the South Island of New Zealand (GNS Science Active Fault Database, http://data.gns.cri.nz/af/). Box shows extent of (b), a location map for the DFDP-1 and AHP boreholes, and field transects. The generalised underlying geology is derived from the GNS Science 1:250000 QMAP project (Rattenbury and Isaac, 2012) and has been draped over a digital elevation model.

860 **Figure 2**

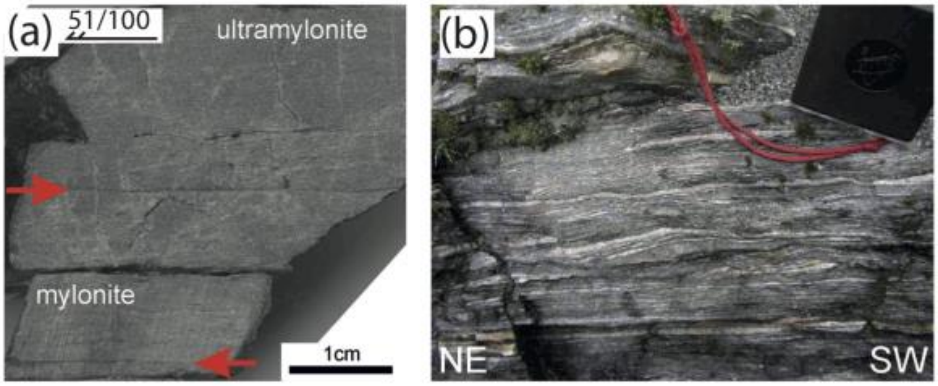

861

862 Figure 2: (a) Quartzofeldspathic Alpine Fault ultramylonite that gradually grades to mylonite at the
863 base of the image. A foliation defined by alternating white quartzofeldspathic bands and dark grey
864 mica bands is hard to distinguish in the ultramylonite, but is more apparent in the mylonite. (b) Well
865 foliated Alpine Fault protomylonite-mylonite transition at Gaunt Creek. Compass is 5 cm wide. Both
866 images previously presented in Toy, (2008).

867

Solid Earth Discuss., https://doi.org/10.5194/se-2017-112
Manuscript under review for journal Solid Earth
Discussion started: 10 October 2017

Figure 3

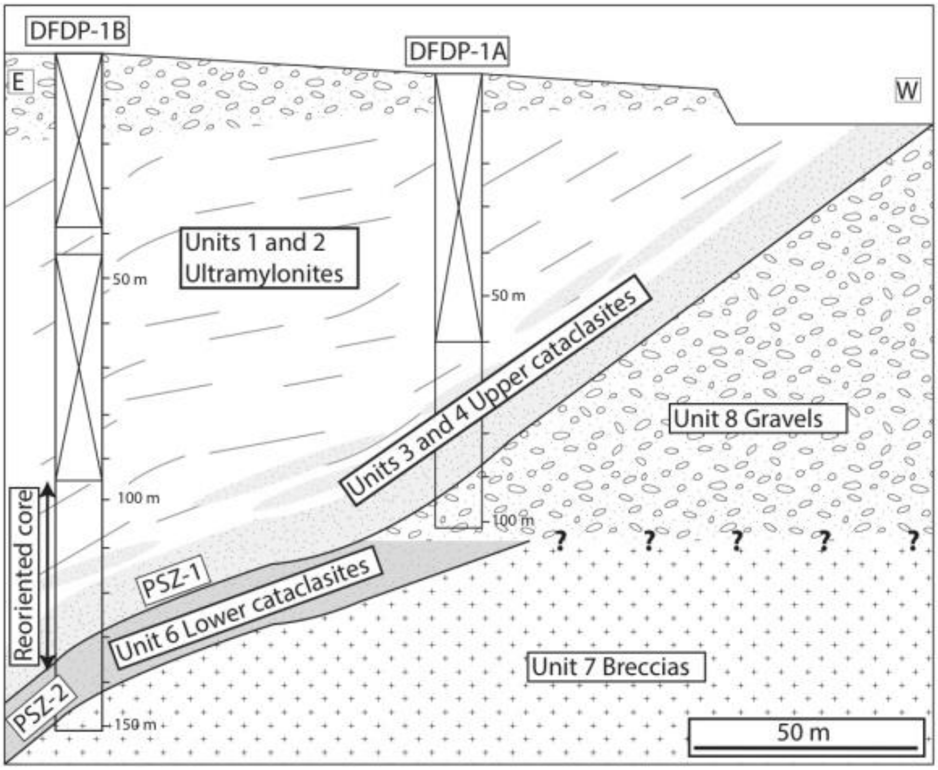

Figure 3: Cross section through the DFDP-1 boreholes, showing interval where reoriented drill-core is located. Boxes with diagonal lines depict intervals in borehole with no core recovery, grey lines represent mylonitic foliation. Modified from Sutherland et al., (2012), with lithological units previously defined by Toy et al., (2015).

Figure 4

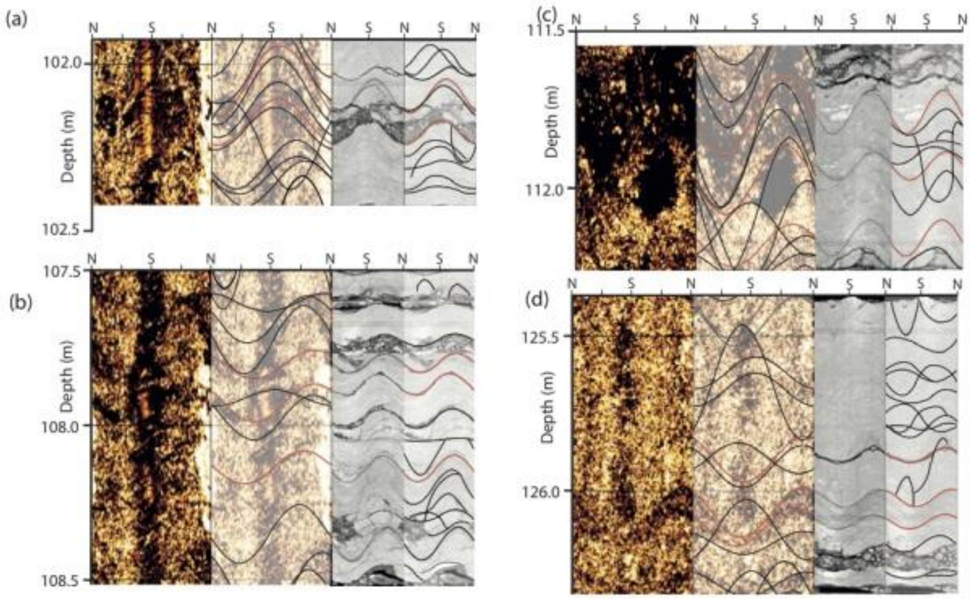

Figure 4: Examples of matching structures between BHTV images and unrolled CT images. In each image, the first two columns are the BHTV amplitude image, without and with interpretations respectively, whilst the third and fourth columns depict the unrolled CT image over the same interval, also without and with interpretations. Fractures that have been traced in red indicate those that were matched to reorientate core.

Figure 5

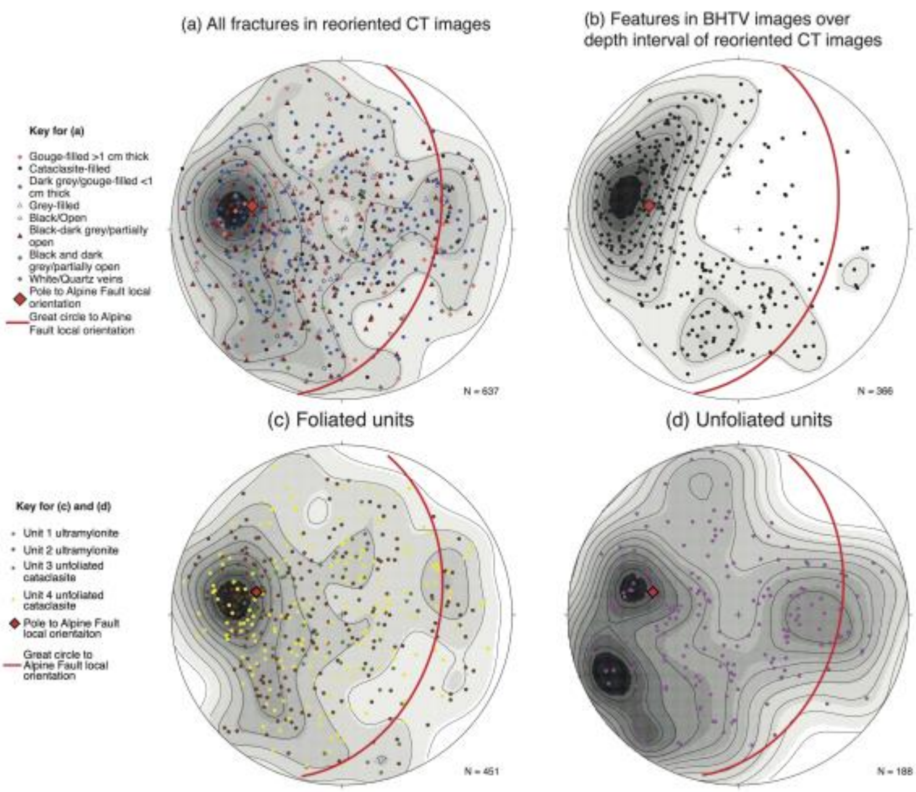

Figure 5: Lower hemisphere equal area stereoplots depicting orientation of fractures in DFDP-1. Contouring on stereoplots was applied to poles that are weighted depending on their orientation correction *w* (see Sect. 3.2), and that are rounded to the nearest whole number. Contours were then generated for the weighted poles using a probability distribution calculated by a Kernel function in the RFOC package for R (Lees, 2014). Great circle represents orientation of Alpine Fault plane and foliation at DFDP-1 site (Townend et al., 2013). (a) Orientation of all fractures that were reoriented by matching structures between unrolled CT images and BHTV images, sorted by fracture type (Williams et al., 2016). (b) Orientation of features recognised in the BHTV images over the interval of reoriented core (94-126 m in DFDP-1B). Fracture orientations extracted from reoriented DFDP-1 CT images in (c) foliated units and (d) unfoliated units, using the DFDP-1 lithological classification scheme (Toy et al., 2015).

Solid Earth Discuss., https://doi.org/10.5194/se-2017-112
Manuscript under review for journal Solid Earth
Discussion started: 10 October 2017

Figure 6

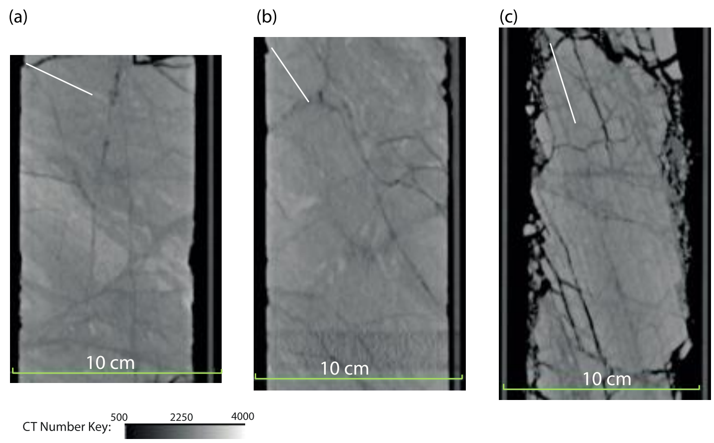

Figure 6: The relationship between foliation and fracture orientations, as observed in 2D CT image slices of DFDP-1 core. In (a) and (b) fractures tend to cross-cut the ultramylonitic foliation (orientation represented by white line in top left corner of each image). (c) Fractures show a greater preference to be aligned parallel to the foliation. Note that (c) was previously shown in Williams et al., (2016), and is not included in the reorientation analysis in Figure 5, as there was no BHTV imagery for this interval. Intervals are (borehole, core section and run, depth interval): (a) DFDP-1A 55-1 75.45-75.62 m, (b) DFDP-1B 35-1 102.49-102.64 m, and (c) DFDP-1B 25-2, 44.80-45.20 m.

Figure 7

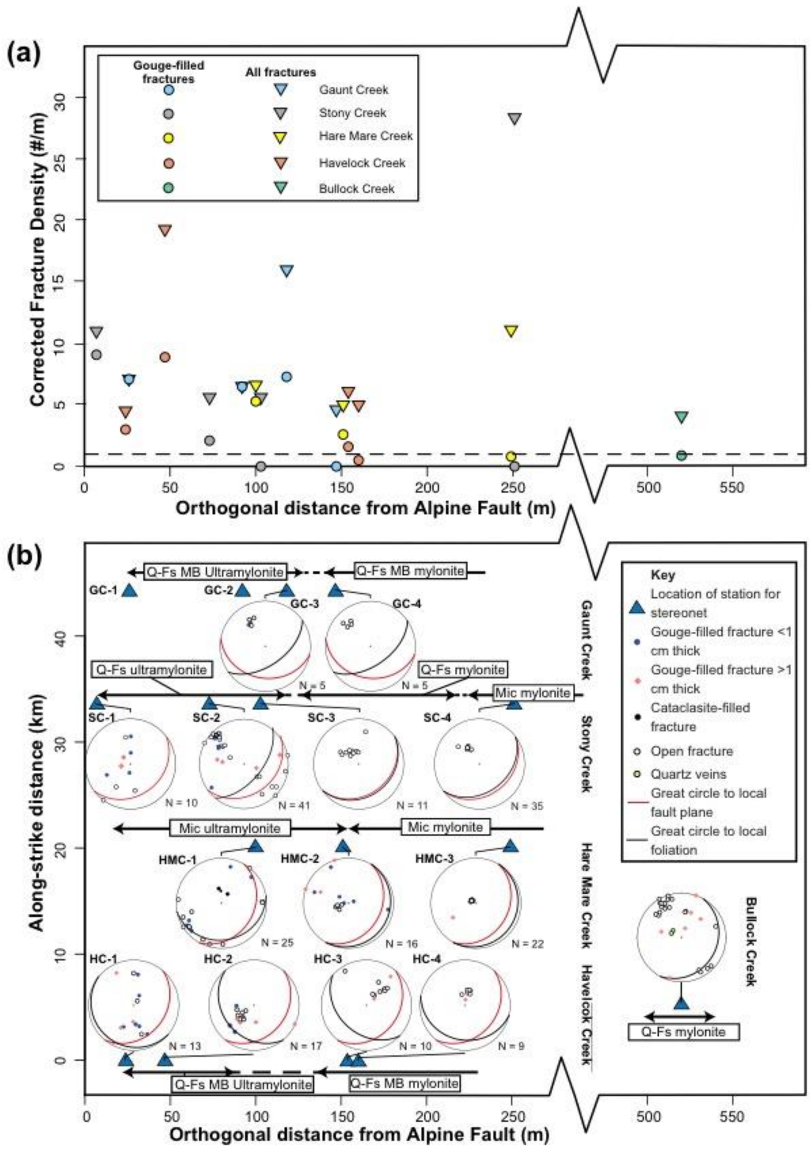

Figure 7: (a) Corrected fracture density at all stations for gouge-filled fractures and all fractures. Dashed line indicates a corrected fracture density of 1 fracture/metre. No orientation data was collected at Gaunt Creek stations 1 and 2, so fracture density is calculated from the two perpendicular transects. (b) Compilation of stereoplots for fracture orientations at each field station. Stations have

Solid Earth Discuss., https://doi.org/10.5194/se-2017-112
Manuscript under review for journal Solid Earth
Discussion started: 10 October 2017

been plotted as a function of distance from the fault and distance along-strike (with respect to Havelock Creek) along within fault rock lithologies. Dashed lines indicate gradational or obscured lithological boundaries. Qfs, Quartzofeldspath; MB, metabasic; Mic, Micaceous. For field cross sections and location of stations, see Figure S1. Results are also summarised in Table S2.

Figure 8

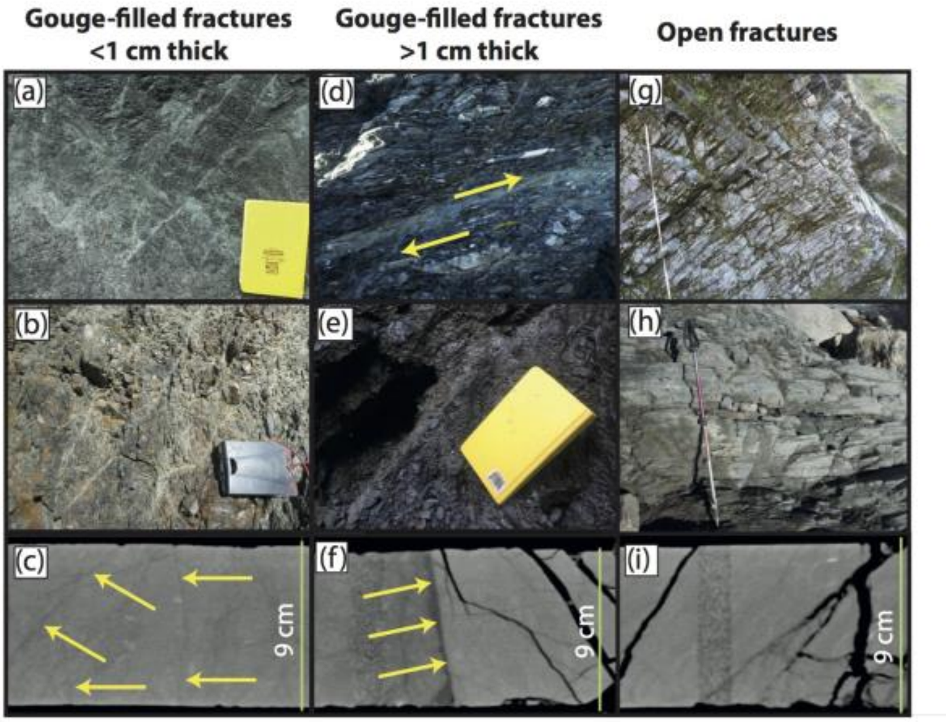

Figure 8: Examples of different fractures observed in the field around the Alpine Fault, and correlative fractures in DFDP-1 CT scans. (a-c) Thin gouge-filled fractures have a range of orientations and found exclusively within 160 m from the fault. They are equivalent to type iii of fractures from Williams et al., (2016). (d-f) Thicker gouge and cataclasite filled fractures are equivalent to type i and ii fractures of Williams et al. (2016) and may be observed at all distances from the Alpine Fault. (g-i) Open fractures are mainly foliation-parallel. Equivalent to type v fractures of Williams et al., (2016). Location of field photos: (a) Waikukupa thrust, (b) and (g) Stony Creek, (d) and (h) Havelock Creek, (e) Bullock Creek. Compass clinometer 8 cm and yellow notebook 20 cm in length. Measuring tape in (e) 1.1 m long, walking pole in (g) 1 m in length. DFDP-1 CT scan intervals: (c) DFDP-1B 56-2 125.35-125.49 m, (f) DFDP-1B 35-1 102.00-102.15 m, (i) DFDP-1B 33-2 99.45-99.60 m

927 **Figure 9**

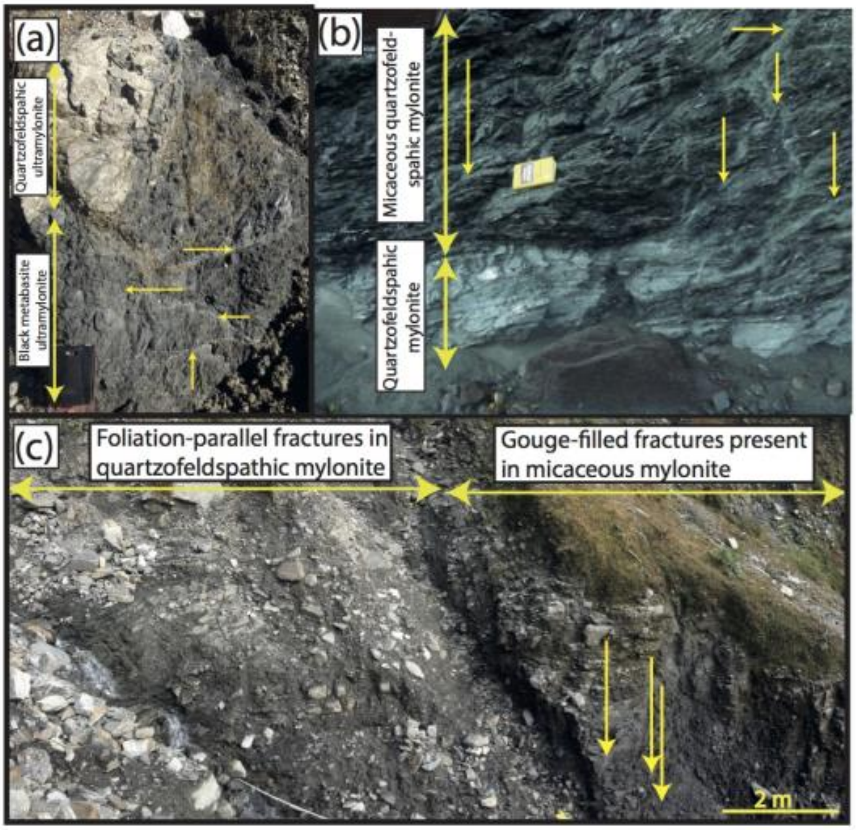

928

929 Figure 9: Field observations of variations in fracture density coincident with lithological diversity. (a
930 & b) Intervals of micaceous and metabasite mylonite containing a relatively high proportion of gouge
931 filled fractures (denoted by yellow arrows) compared to interlayered quartzofeldspathic mylonite. (c)
932 Transition from micaceous mylonite to quartzofeldspathic mylonite coincides with furthest extent of
933 intensive gouge-filled fracturing. Taken at (a) Gaunt Creek, (b) Havelock Creek, (c) Hare Mare Creek.
934 Compass clinometer 8 cm and yellow notebook 20 cm in length.

Figure 10

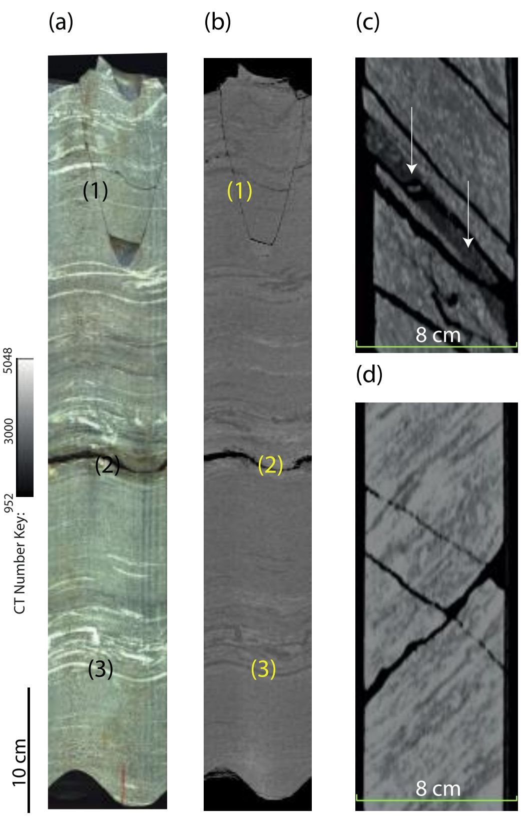

Figure 10: Fracture styles noted in the Amethyst Hydro Project (AHP) drill-core. Unrolled images of AHP drill-core (BH1 45-2 124.3-124.9 m) taken by (a) DMT core scanner and (b) generated from a CT image. (1) Identifies fracture cutting across foliation, (2) foliation-parallel fracture with alteration halo, (3) foliation defined by quartzofeldspathic bands that have low CT numbers. (c&d) Core-axial parallel CT image slices of AHP drill-core. In (c) white arrows point to a 'crush zone' sub parallel to foliation (BH2 75-2 155.92-156.04 m). (d) more variable fracture orientations identified in BH4 (Section 70-4 196.62-196.80 m).

Solid Earth Discuss., https://doi.org/10.5194/se-2017-112
Manuscript under review for journal Solid Earth
Discussion started: 10 October 2017

Figure 11

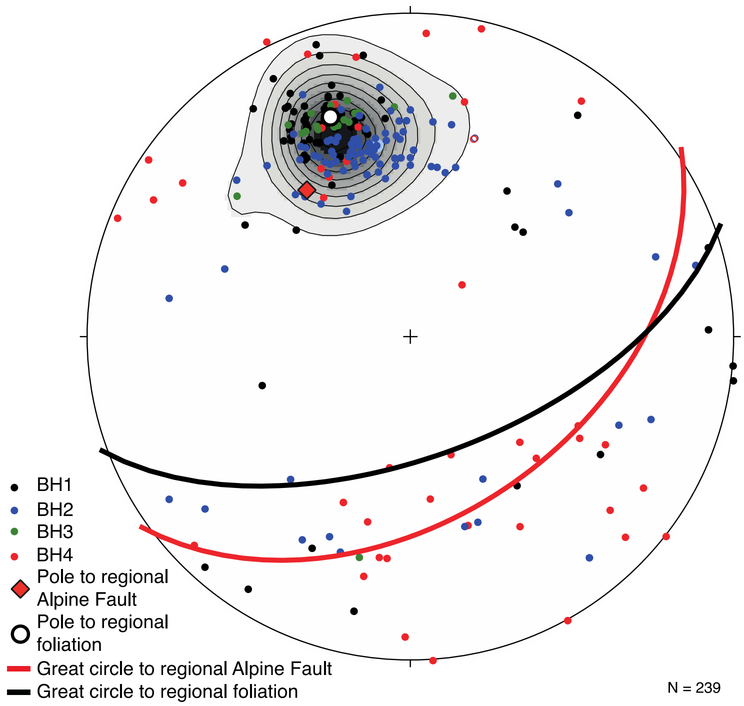

Figure 11: Equal area, lower hemisphere projection of fracture orientations recognised in CT scans of AHP drill-core separated by borehole. Contours plotted with weighted poles (see Figure 5).

Figure 12

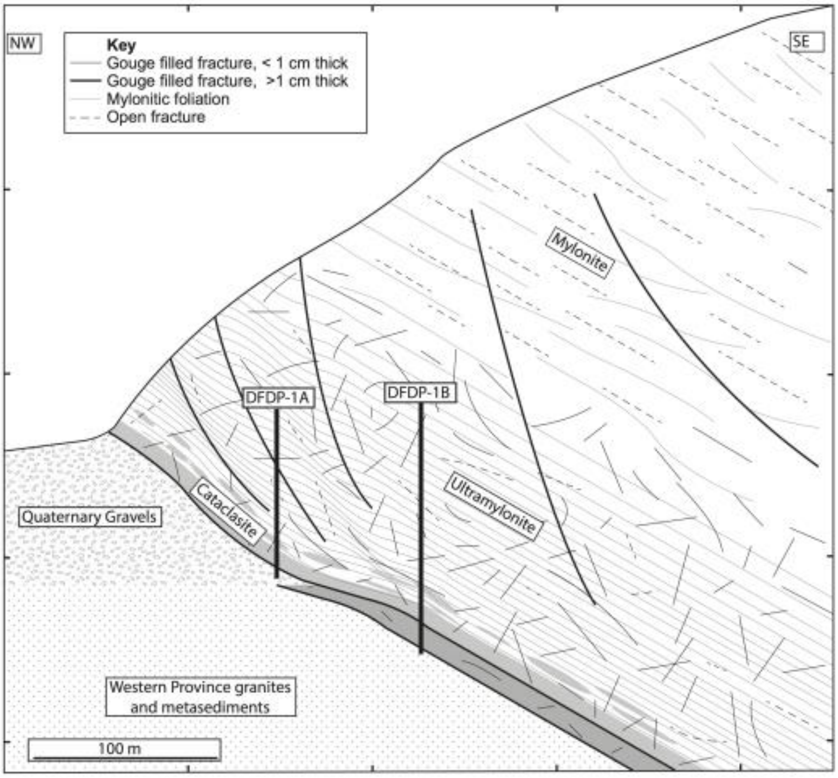

Figure 12: A schematic cross section through a thrust section of the central section of the Alpine Fault, depicting fracture network, its relationship to foliation, and the distribution of subsidiary faults. Respective position of DFDP-1 boreholes also shown. Constructed from cross sections previously presented in Norris and Cooper, (2007) and Sutherland et al., (2012).

Solid Earth Discuss., https://doi.org/10.5194/se-2017-112
Manuscript under review for journal Solid Earth
Discussion started: 10 October 2017

Figure 13

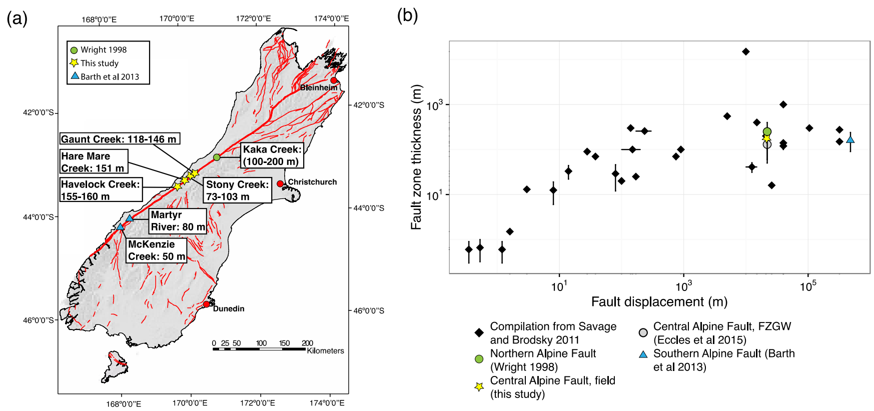

Figure 13: (a) Compilation of estimates of the extent of intensive gouge-filled fracturing on the Pacific Plate side of the Alpine Fault from four creek sections in this study (Gaunt Creek, Stony Creek, Hare Mare Creek and Havelock Creek), which is considered to be the best indicator of Alpine Fault damage zone width. This is combined with other along-strike estimates of damage zone thickness for the Alpine Fault: McKenzie Creek and Martyr River (Barth et al., 2013) and Kaka Creek (Wright, 1998). (b) Log-log plot of fault zone thickness as a function of fault displacement previously presented in Savage and Brodsky, (2011), combined with estimates made for the Alpine Fault assuming footwall damage is no more extensive than in the hanging-wall. Displacement for the Alpine Fault is 480 km (Norris and Cooper, 2007; Wellman, 1953), However, convergence along the Alpine Fault's central section requires that it erodes its own fault rocks so these points are plotted to reflect only the brittle displacement the rocks themselves have accommodated as they are exhumed through the seismogenic zone (22 km, Barth et al., (2012)). Error bars reflect uncertainty in constraining fault zone width (as for example, footwall damage is largely unknown), not necessarily variability in fault zone thickness.

Solid Earth Discuss., https://doi.org/10.5194/se-2017-112
Manuscript under review for journal Solid Earth
Discussion started: 10 October 2017

Figure A1

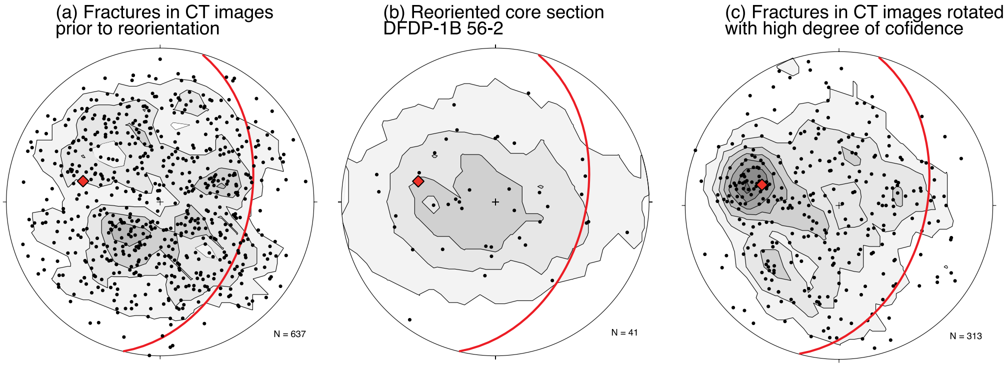

Figure A1: Stereoplots to tests the confidence in reorientations applied to rotate DFDP-1 CT scan fracture orientations into geographic coordinates. Red great circle and diamond in each plot represents plane and pole to the Alpine Fault orientation measured in DFDP-1B. Plotted with Kamb contours with intervals of two standard deviations. (a) Orientation of fractures shown in Figure 5a before rotation, (b) orientation of reoriented fractures within a single core section (DFDP-1B 56-2), and (c) orientation of fractures in CT images from core sections that were oriented with a high degree of confidence with BHTV images.